Polym. Bull. (2012) 68:151–165
DOI 10.1007/s00289-011-0546-4

ORIGINAL PAPER

Structural and thermal degradation studies on thin films of the nanocomposite system PVP–$Ce(SO_4)_2 \cdot 4H_2O$

Ahmad-Fouad Basha · Mohammad A. F. Basha

Received: 2 May 2011 / Revised: 5 June 2011 / Accepted: 5 June 2011 /
Published online: 14 June 2011

Abstract Newly prepared and well-characterized nanocomposite thin films of polyvinylpyrrolidone (PVP) containing 2, 5, 10, and 15 wt% cerium (IV) sulfate have been subjected to structural and thermal stability investigations using the transmission electron microscopy (TEM), atomic force microscope (AFM), X-ray diffraction (XRD), differential scanning calorimetry (DSC), and thermogravimetric analysis (TGA). The nanostructural nature of the investigated films was confirmed from the estimated average size of the particles. Better crystallinity was achieved with the addition of 15 wt% cerium disulfate to PVP. The thermograms of DSC and its derivative for the investigated composites indicated the development of a new endothermic peak of decomposition nature, and the values of peak position and associated enthalpy were found to be composition dependent, indicating a decrease in thermal stability of PVP with the increase of dopant concentration. Thermograms of TGA and its derivative revealed that the weight loss in the composite samples is composition dependent, and two main steps of degradation were clearly evident, the first assigned mainly to dehydration processes at relatively lower temperature range (30–200 °C) and the second at higher temperatures up to 400 °C attributed to decomposition processes. Thermodynamic parameters, such as activation energy, entropy, enthalpy, and Gibbs free energy, were also determined on the basis of thermogravimetric data.

Keywords Polyvinylpyrrolidone · Cerium disulfate · Magnetic nano-composites

A.-F. Basha · M. A. F. Basha (✉)
Physics Department, Faculty of Science, Cairo University, Giza, Egypt
e-mail: mafbasha@gmail.com

A.-F. Basha
e-mail: afbasha@gmail.com
URL: www.afbasha.com

Abbreviations

PVP	Polyvinylpyrrolidone
TEM	Transmission electron microscopy
AFM	Atomic force microscope
XRD	X-ray diffraction
DSC	Differential scanning calorimetry
TGA	Thermogravimetric analysis
NMR	Nuclear magnetic resonance
IR	Infrared

Introduction

Numerous polymeric composites generally consist of a polymer continuous phase surrounding a dispersed phase in combination, with the aim of improving the properties of the component materials and developing hybrid materials with unique properties. Homogeneity increases as the size of the dispersed phase is reduced, and the nanocomposite is formed when the dispersed phase can reach the nanoscale ($\leq 10^{-7}$ m). Such hybrids which contain nanoparticles with high surface area and small particle size are of certain interest due to their widely spread applications as, for example, catalytic agents, luminescent materials, and electrochemical devices [1–6].

In this respect, the polymeric nanocomposite systems containing rare-earth metal salts belong to a recently advancing branch of an increasing importance in contemporary polymer science and technology [5–8]. The resulting magnetic nanostructures are quite remarkable materials because they exhibit exclusive functionalities originated from both polymer and inorganic additives. Such materials find promising applications in the fabrication of plastic lasing devices and information storing media [5, 9–12]. In fact, doping of transition metal salts with different concentrations into polymers can produce pronounced changes in various properties of complexes and lead to the development of materials with tailor-made properties [3, 7, 8, 13–15].

In recent publication for one of the present authors [16], a systematic research work has been started to prepare and characterize the new nanocomposite systems PVP–$GdCl_3$ and PVP–$HoCl_3$. In another work [17], the author reported that the nanocomposites PVP–$Ce(SO_4)_2{\cdot}4H_2O$ were found to display very good film-forming properties, and their miscibility along with complex formation were elucidated using nuclear magnetic resonance (NMR) and infrared (IR) spectroscopy. Magnetic and optical characterization studies were also performed.

The components of the composites studied in the present work were polyvinyl-pyrrolidone (PVP) and tetrahydrated cerium (IV) disulfate, $Ce(SO_4)_2{\cdot}4H_2O$. The pyrrolidone rings in PVP contain a proton accepting carbonyl moiety and prefer to complex with many inorganic salts, while $Ce(SO_4)_2{\cdot}4H_2O$ is usually used as highly active oxidant in the synthesis of polymers. However, investigations of the cerium

(IV) disulfate complete structure and its thermal degradation revealed an obvious disagreement among different references [18–25].

Unfortunately, to the best of our knowledge, the literature is almost devoid of any data concerning the study of the physical properties of nanocomposite system PVP/$Ce(SO_4)_2{\cdot}4H_2O$, among which the issue of thermal degradation and stability is essentially of both scientific interest and technological importance [23].

The aim of the present study is to investigate the structure and thermal stability of PVP films in the presence of small amounts (2, 5, 10, and 15 wt%) of ceric sulfate and to determine some characteristic structural and thermodynamical parameters of PVP, $Ce(SO_4)_2{\cdot}4H_2O$ and their nanocomposites.

Experimental

Materials

PVP with FW $\sim$40,000 was supplied by GFS chemicals, Powell, OH. The transition metal salt cerium disulfate with empirical formula $Ce(SO_4)_2{\cdot}4H_2O$, FW 404.30, and purity 99.9% was supplied by Strem Chemicals Inc., Newburyport, MA.

Sample preparation

The solution method was used to obtain film samples. A known amount of PVP granules was dissolved in doubly distilled water to prepare a clear solution. Also, known amount of $Ce(SO_4)_2{\cdot}4H_2O$ salt was dissolved in small amount of distilled water containing few drops of 0.1 M H_2SO_4 at room temperature. Solutions of $Ce(SO_4)_2{\cdot}4H_2O$ and PVP were mixed together with different weight percentages, 2, 5, 10, and 15 wt% of $Ce(SO_4)_2{\cdot}4H_2O$, using a magnetic stirrer, at 50 °C on a water path for several hours in order to obtain complete dissolution. Samples with higher dopant concentrations were difficult to obtain because of the limited solubility of $Ce(SO_4)_2{\cdot}4H_2O$ in water (36 g L^{-1}, at 50 °C). Thin films of appropriate thickness ($\sim$80 μm) were cast onto glass Petri dishes and then dried in air at room temperature for about 7 days until the solvent was completely evaporated.

Measuring techniques

Morphological investigations were performed using a transmission electron microscope of the type Jeol JEM-1230 (Jeol Ltd, Tokyo, Japan) at a working voltage of 100 keV.

A drop of the sample was placed onto a carbon-coated copper grid followed by drying at room temperature.

Images were recorded under an axial illumination at approximate nanoscale focus. The diameter of the objective aperture used was 1 μm. The particle size distribution was determined for more than 300 particles of diameters up to 100 nm along a fixed direction on the micrograph.

Topographic imaging of representative sample was performed at room temperature and atmospheric pressure using an Atomic force microscope (model SPM-9600 manufactured by Shimadzu Corporation, Kyoto, Japan) in contact mode.

The X-ray diffraction (XRD) patterns were obtained with Panalytical X'PERT-PRO. Target: Cu K_α radiation with 2nd monochromotor, 40 mA, 45 kV, made in Holand.

Thermal analysis was carried out using computerized differential scanning calorimeter (DSC) and thermogravimetric analysis (TGA) instruments (TA-50) manufactured by Shimadzu Corporation (Kyoto, Japan) under an atmosphere of nitrogen at a flow rate of 30 ml/min. The heat rate used for all samples under investigation was 10 °C/min.

Results and discussion

Transmission electron microscopy (TEM)

Figure 1 shows a typical TEM overview of the nanoparticles in the sample PVA + 10% $Ce(SO_4)_2{\cdot}4H_2O$. It can be seen that the additive salt is uniformly dispersed in the PVP matrix, and the sample under investigation is nanostructured material. Statistical results revealed that the value of the average particle size is mostly about 45 nm. The figure also shows that the shape of the particles appears nearly spherical. Agglomerated particles, as well as separated ones are present in the figure. Figure 1 shows also the histogram of the particles size distribution.

Mainly, the agglomeration can be partly attributed to some extent to electrostatic or Van der Waals' forces between particles. Also, the nanoparticles containing cerium ions tend to agglomerate because of their permanent magnetic moment [16, 26]. Hence, the particles are permanently magnetized and get agglomerated.

Atomic force microscopy (AFM)

Figure 2 also shows representative topographic AFM image for the composite PVP film containing 10 wt% $Ce(SO_4)_2{\cdot}4H_2O$, where the nanostructural nature is clearly evident with calculated values of 45 nm for average particle size, 0.003 μm^2 for average surface area, and 0.55 nm for average surface roughness. Such parameters effectively play an important role in the contact area of interaction between the bodies, particularly in the nanoscale [27].

X-ray diffraction (XRD)

Figure 3 shows the X-ray diffraction patterns of the materials PVP and $Ce(SO_4)_2{\cdot}4H_2O$, together with the composites PVP + 5 wt% $Ce(SO_4)_2{\cdot}4H_2O$, PVP + 10 wt% $Ce(SO_4)_2{\cdot}4H_2O$, and PVP + 15 wt% $Ce(SO_4)_2{\cdot}4H_2O$. Figure 3a shows two diffuse halos observed for PVP over the angular ranges 9°–15° and 15°–35°, with maximum counts at 11° and 21°, respectively. This indicates the amorphous nature of the PVP structure as previously reported in literature [18].

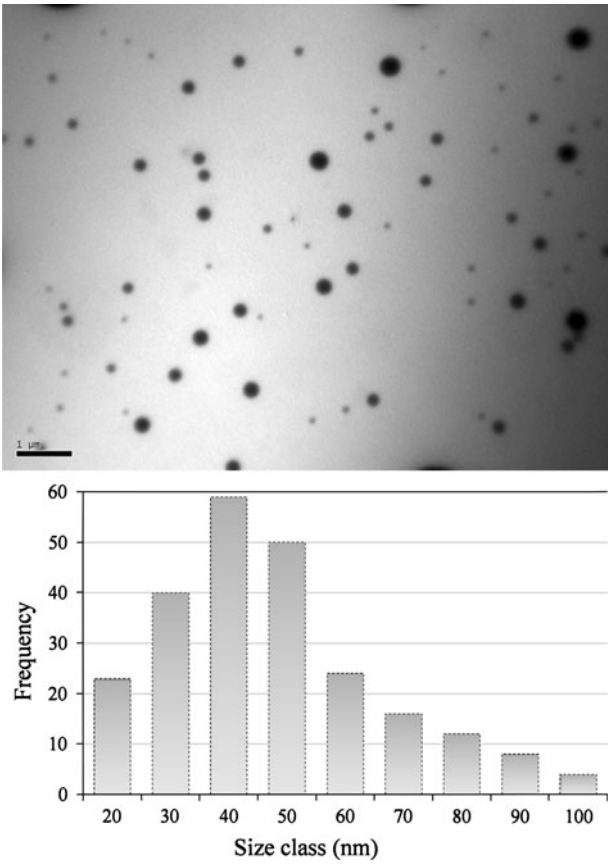

Fig. 1 TEM image of the composite PVP + 10 wt% $Ce(SO_4)_2{\cdot}4H_2O$ and the corresponding histogram of the particle size distribution

However, Nishio et al. [20] reported two broad rings at 11.7° and 19.8° in the diffraction pattern of PVP film. They assumed that some crystalline ordering is also present in the homopolymer film. Presumably, the outer diffuse ring in the WAXD pattern may be identified with an amorphous halo, while the inner diffraction ring, located at $2\theta = 11.7°$ with relatively greater intensity, originates from a phase of low regularity. In this phase, PVP molecules are arranged with chain-to-chain lateral ordering to assume a pseudohexagonal packing, but without any definite longitudinal repeat spacing.

Figure 3e presents also the powder diffraction pattern and crystallographic data obtained in the present work for the tetrahydrated cerium disulfate compound. The interplaner spacing (d_{hkl}) values, labeled on the corresponding Bragg reflections of the obtained diffractogram, were compared to that previously reported in the database, and the best fit matching most of the experimental peaks was achieved with the calculated pattern of the monoclinic $Ce(SO_4)_2{\cdot}4H_2O$ with space group C2/c [28]. This fitting is an evidence of a pure material. Once again, we remained that the

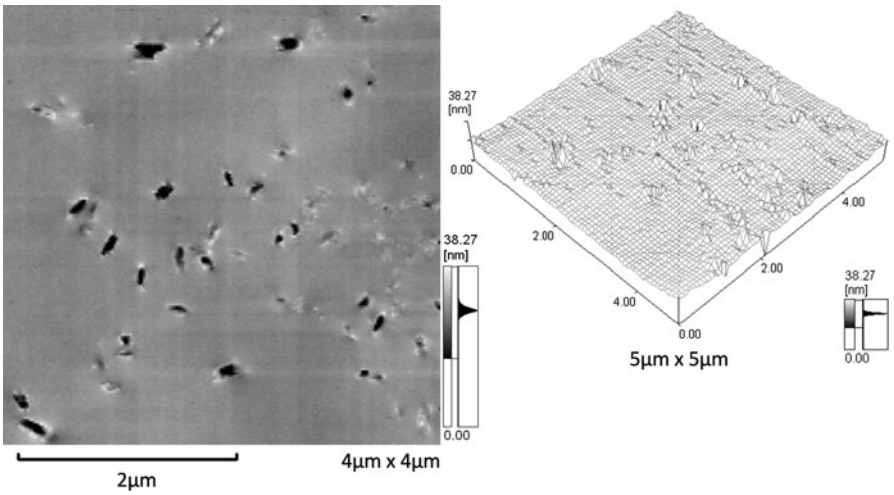

Fig. 2 AFM images of the sample PVP + 10 wt% $Ce(SO_4)_2{\cdot}4H_2O$

complete crystal structure determination of $Ce(SO_4)_2{\cdot}4H_2O$ is still ambiguous in the literature [24, 25, 28, 29].

Addition of $Ce(SO_4)_2{\cdot}4H_2O$ dopant until a concentration of 5% by weight to PVP did not entail remarkable change in the diffractogram of the amorphous PVP, except some increase in intensity of the halo at 21° and vanishingly small intensity of the halo at 11°, as illustrated in Fig. 3b. When the dopant content reached 10 wt%, a new diffraction profile of crystalline phase was easily discernible. The composite PVP + 10 wt% $Ce(SO_4)_2{\cdot}4H_2O$, Fig. 3c, confirmed a good crystallinity for this material. The appearance of the hump at $2\theta = 21°$ indicates that the amorphous phase of PVP is still present. Better crystallinity was achieved with a highly possible addition of 15 wt% cerium compound to PVP, Fig. 3d. The limited solubility of cerium (IV) sulfate tetrahydrate in water restricted the use of higher dopant concentrations [30].

The average size of the nanocomposite particles (D_{hkl}) was estimated from the X-ray diffraction pattern, Fig. 3, using the well-known Sherrer formula [31]

$$D_{hkl} = 0.98\frac{\lambda}{\beta_{hkl}\cos(\theta_{hkl})}, \tag{1}$$

where λ is the wavelength of the X-rays (0.154056 nm), β_{hkl} is the full width at half maximum (FWHM) of the diffraction peak, and θ_{hkl} is the Bragg diffraction angle.

The calculated values of average size (diameter) of the particles in the composites 10 wt% $Ce(SO_4)_2{\cdot}4H_2O$ + PVP and 15 wt% $Ce(SO_4)_2{\cdot}4H_2O$ + PVP were found to be 29 and 32 nm, respectively, i.e., within the range of the nanoscale. These values of nanoparticles size are in good conformity with the values calculated from TEM and AFM images.

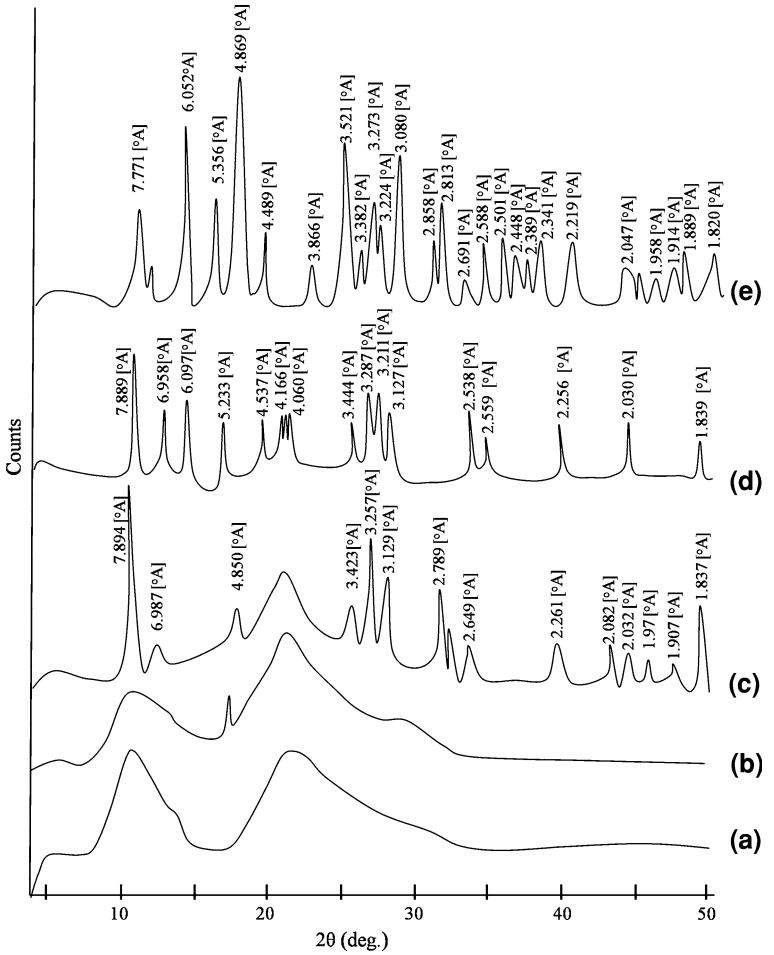

Fig. 3 X-ray diffraction pattern for (*a*) pure PVP, (*e*) pure $Ce(SO_4)_2{\cdot}4H_2O$ and (*b–d*) for the composites containing 5, 10 and 15 wt% $Ce(SO_4)_2{\cdot}4H_2O$-doped PVP, respectively

Thermal properties

Differential scanning calorimetry (DSC)

Figure 4 shows DSC and its derivative thermograms obtained at a heating rate of 10 °C/min for pure PVP, pure $Ce(SO_4)_2{\cdot}4H_2O$, and their composites during a first heating scan. For pure phase of PVP, Fig. 4a, the curves of DSC and its derivative show a major endothermic peak centered at about 72 °C, assigned to a glass transition process associated with an enthalpy of 542.35 J/g, and extending from about 30–125 °C. It is probable that this broad peak includes another small one at 100 °C due to the removal of some water trapped in the polymeric network. Making use of the method of water contribution subtraction [32], Fig. 4 shows the corrected

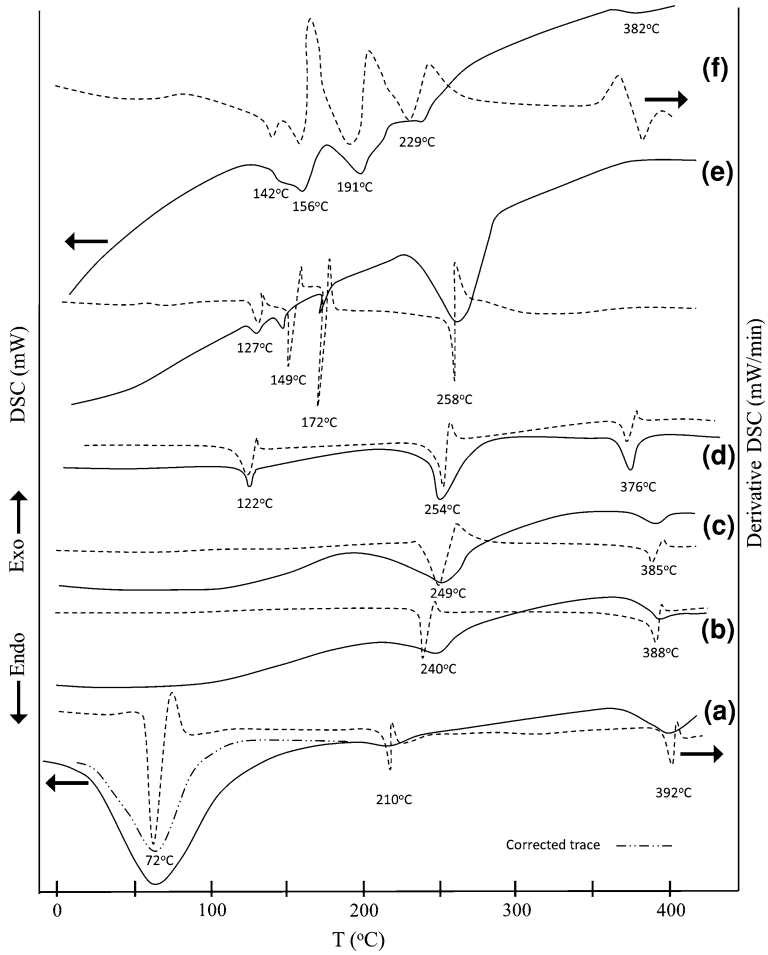

Fig. 4 DSC and its derivative thermograms for (*a*) pure PVP, (*f*) pure $Ce(SO_4)_2{\cdot}4H_2O$ and (*b*–*e*) for the composites containing 2, 5, 10 and 15 wt% $Ce(SO_4)_2{\cdot}4H_2O$-doped PVP, respectively

trace corresponding to the PVP sample after subtracting the water effect. The broad glass transition is apparently a result of the nonuniform nature of this process.

In the literature, several conflicting values of glass transition temperature (T_g) of PVP were found, ranging from 42.5 °C at a scanning rate of 8 °C/min to 177 °C at a heating rate of 25 °C/min [18, 33–37]. Several reasons are usually suggested for such confliction of T_g values including: presence of impurities, changes in specific heat involved, inability to attain near-equilibrium conditions during measurement, and/or the faster rate of temperature change compared to the change in molecular rearrangement, along with the large influence of sorbed moisture due to the hygroscopic nature of the material [18, 37].

The minor endothermic peak at about 210 °C in the thermograms of DSC and its derivative for PVP may be attributed to a solid–solid transition of unspecified

nature. Kumar et al. [18] reported a similar peak at 206 °C and found, using a hot stage microscope, that PVP showed off-white to light yellow coloration at about 246 °C.

In addition to the endotherms at 72 and 210 °C, the PVP sample showed an endothermic peak at about 392 °C, which can be attributed to the thermal chemical decomposition process associated with an enthalpy of 16.94 J/g.

It is to be mentioned that, in a subsequent cooling and reheating runs, the endothermic peaks have been disappeared, indicating the irreversibility of thermograms of both DSC and its derivative for pure PVP.

On the other hand, Fig. 4f shows also the DSC and its derivative thermograms for the pure compound $Ce(SO_4)_2{\cdot}4H_2O$. The endothermic dehydration peaks at 142, 156, and 191 °C are associated with enthalpies of 2.52, 17.69, and 61.17 J/g, respectively. The peaks centered at about 229 and 382 °C are probably of thermal decomposition nature associated with enthalpies of 25.15 and 12.52 J/g.

Figure 4b–e depicts the DSC and its derivative curves for the composite samples under investigation and the obtained data are summarized in Table 1. One can observe that the addition of 2 wt% $Ce(SO_4)_2{\cdot}4H_2O$ to PVP entailed a development of a new characteristic endothermic peak at 240 °C with an enthalpy of 49.17 J/g. The increase of dopant concentration led to a shift of the peak position toward higher temperature, along with a remarkable gradual increase of enthalpy values. Besides, the endothermic peak assigned to thermal decomposition of PVP at 392 °C can be observed to exhibit gradual decrease toward lower temperatures together with considerable increase of corresponding enthalpies, indicating a remarkable decrease in the thermal stability of PVP with the increase of dopant concentration. It is to be mentioned also that the peak at 72 °C for PVP disappeared in the thermograms of the investigated composites.

Table 1 Endothermic peak temperatures (T_p) and associated enthalpies (ΔH) for PVP, $Ce(So_4)_2{\cdot}4H_2O$ and their nanocomposites as obtained from the thermograms of DSC and its derivative

Specimen	Endothermic peak temperatures (T_p) and associated enthalpies (ΔH)					
	Peaks in the region 30–200 °C		Peaks in the region 200–300 °C		Peaks in the region 300–400 °C	
	T_p (°C)	ΔH (J/g)	T_p (°C)	ΔH (J/g)	T_p (°C)	ΔH (J/g)
PVP	72	542.35	210	0.63	392	16.94
PVP + 2% $Ce(SO_4)_2{\cdot}4H_2O$	–	–	240	49.17	388	22.63
PVP + 5% $Ce(SO_4)_2{\cdot}4H_2O$	–	–	249	129	385	46.87
PVP + 10% $Ce(SO_4)_2{\cdot}4H_2O$	122	2.02	254	180.13	376	95.1
PVP + 15% $Ce(SO_4)_2{\cdot}4H_2O$	127	4.55	258	219.85		
	149	4.41			–	–
	172	3.87				
$Ce(SO_4)_2{\cdot}4H_2O$	142	2.52	229	25.15	382	12.52
	156	17.69				
	191	61.17				

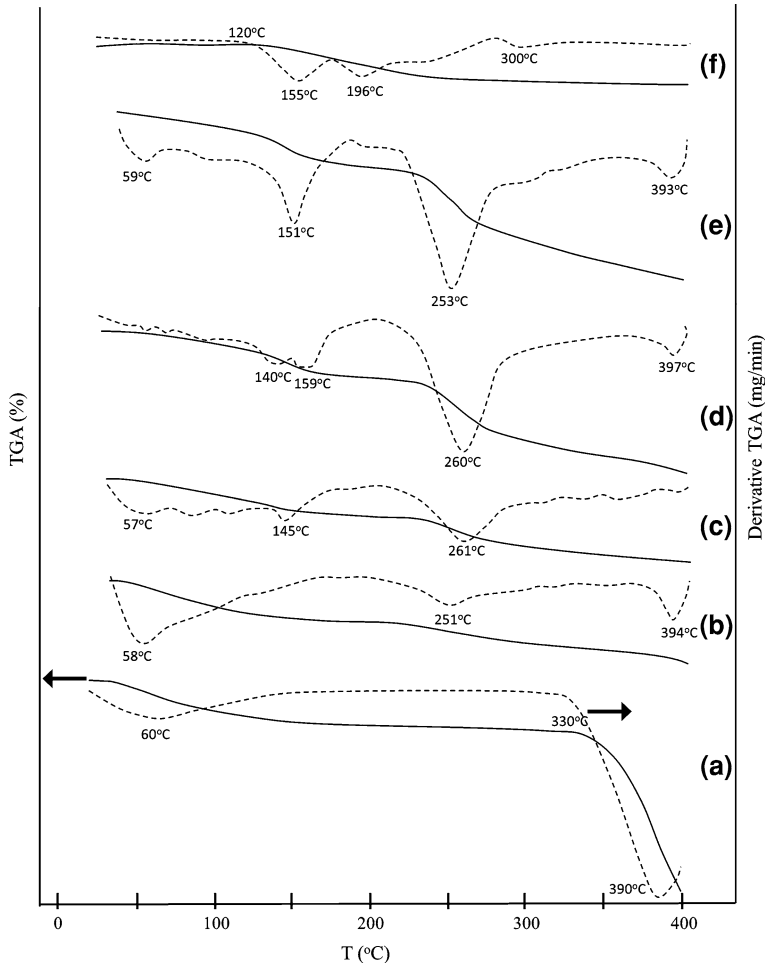

Fig. 5 TGA and its derivative thermograms for (*a*) pure PVP, (*f*) pure $Ce(SO_4)_2{\cdot}4H_2O$ and (*b*–*e*) for the composites containing 2, 5, 10 and 15 wt% $Ce(SO_4)_2{\cdot}4H_2O$-doped PVP, respectively

Thermogravimetric analysis (TGA)

To determine the stability of the pure PVP film and the effect of dopant concentration on this stability, measurements of TGA and its derivative were carried out in the temperature range 30–400 °C, and the obtained data were presented in Fig. 5. The initial and final temperatures of degradation steps, and the percentages of weight loss were determined from the TGA curves, and the maximum temperature of the highest rate of weight loss for each degradation step (T^*_{max}) was determined from the derivative of TGA curves. The obtained data from Fig. 5 are summarized in Table 2.

Figure 5 and Table 2 show that PVP is thermally stable over a wide temperature range (115–330 °C), and two distinct steps of degradation were clearly evident. The

Table 2 Stages of degradation, % weight loss and thermodynamic parameters for PVP, $Ce(SO_4)_2{\cdot}4H_2O$ and their nanocomposites, as obtained from thermogravimetric analysis

Samples	Temperature (°C)				% Weight loss		Thermodynamical parameters			
	Start	End	T^*_{max}		Partial	Total	$E^{\#}$ (kJ/mol)	$\Delta S^{\#}$ (J/K/mol)	$\Delta H^{\#}$ (kJ/mol)	$\Delta G^{\#}$ (kJ/mol)
PVP	30	115	60		11.2	75.6	36.16	−216.43	33.29	107.69
	330	400	390		64.37		54.15	−364.34	1.15	176.48
PVP + 2% $Ce(SO_4)_2{\cdot}4H_2O$	30	150	58		15.58	33.7	28.07	−246.50	25.05	113.85
	150	400	251	394	18.12		36.16	−271.05	31.60	217.76
PVP + 5% $Ce(SO_4)_2{\cdot}4H_2O$	30	160	57	145	14.67	36.7	30.48	−245.28	27.42	134.85
	160	400	261		22.00		43.81	−253.65	39.21	163.79
PVP + 10% $Ce(SO_4)_2{\cdot}4H_2O$	30	175	140	159	15.57	51.1	30.33	−250.31	27.21	140.47
	175	400	260	397	35.56		53.75	−236.54	49.09	212.59
PVP + 15% $Ce(SO_4)_2{\cdot}4H_2O$	30	180	59	151	17.03	56.5	28.21	−257.31	25.06	141.04
	180	400	253	393	39.43		52.47	−238.67	47.79	212.26
$Ce(SO_4)_2{\cdot}4H_2O$	120	200	155	196	5.28	14.8	56.98	−190.73	53.38	146.82
	200	400	300		9.53		20.52	−295.62	15.75	160.35

T^*_{max}, the peak temperature of the maximum rate of degradation processes as obtained from the derivative of TGA curves

mass loss of the first step starts at 30 °C and reaches to maximum at 60 °C, while the relatively much larger mass loss of the second step starts at about 330 °C and reaches to maximum at about 390 °C, and the total percentage of weight loss amounts to 75.6%. The first degradation stage includes the process of glass phase transition, together with dehydration process of residual water associated with the sample. Due to the hydrophilic nature of PVP, water can be absorbed from the atmosphere and constitutes a significant weight loss percentage which can be identified in the first mass-loss event in the TGA trace. On the other hand, the second major decomposition step is thought to include mainly a chemical degradation process resulting from bond scission in the polymer backbone.

Concerning the compound $Ce(SO_4)_2{\cdot}4H_2O$, one can see from Fig. 5f and Table 2 that this compound is thermally stable over the temperature range from about 30 to 120 °C, showing much less temperature range of stability than PVP. Two main degradation steps appeared successively: the first one starts at about 120 °C and its mass loss reaches to maximum at 155 and 196 °C, while the second one starts at 200 °C and its mass loss reaches to maximum at 300 °C. The percentage mass loss in the first stage amounts to 5.28%, while that of the second step amount to 9.53%. This means that the first degradation step is mainly a dehydration process, while the second one is mainly a decomposition process, within the temperature range employed (30–400 °C).

Unfortunately, the description of the thermal behavior and decomposition of tetrahydrated ceric sulfate is obviously contradictory in literature. An early study reported that this compound already decomposes into $3CeO_2{\cdot}4SO_3$ at 195 °C, while

other studies showed that $Ce(SO_4)_2{\cdot}4H_2O$ decomposes in four stages, losing two molecules of water in the first and second stages, resulting in the formation of anhydrous $Ce(SO_4)_2$ at 340 °C, then $Ce(SO_4)_2$ converts into $CeO_2{\cdot}2Ce(SO_4)_2$ which in the final stage, between 700 and 940 °C loses sulfur dioxide and oxygen to give CeO_2 [24, 38]. In contrast, other authors showed evidence that the dehydration process starts at 98 °C and proceeds in two steps up to 322 °C. Further, they suggested that the observed weight loss in the range 450–495 °C corresponds to the reduction of anhydrous cerium (IV) sulfate, giving $Ce_2(SO_4)_3$, SO_2, and O_2 [39, 40]. Accordingly, tedious work is still needed from crystallographers in order to unfold this contradiction.

Figure 5b–e presents the TGA and its derivative curves for the composite samples under investigation, and the obtained data are listed in Table 2. It can be noted that TGA and its derivative curves of all composite samples had continuous weight loss up to 400 °C, and the composite containing 2 wt% $Ce(SO_4)_2{\cdot}4H_2O$ had the smallest weight loss among all composites. The presence of $Ce(SO_4)_2{\cdot}4H_2O$ appears to cause an earlier degradation onset than that in the pure polymer. This means that PVP is less thermally stable in the presence of 2–15 wt% of cerium disulfate. The temperature of maximum rate of weight loss for PVP is higher than those for $Ce(SO_4)_2{\cdot}4H_2O$ within the temperature range of measurements.

The weight loss in the composite samples is generally less than that in pure PVP and greater than that in cerium disulfate tetrahydrate, but it exhibits a gradual increase with increase of dopant concentration. Holmes et al. [23] reported similar trend on studying the pyrolysis behavior of TiO_2–PVP composite materials. Besides, it was reported for some rare-earth metal salts doped polyethylene oxide that vaporization of residual water was observed to occur in the temperature range 40–150 °C [5]. Moreover, the water of coordination is usually eliminated throughout the temperature range 100–350 °C, and this process is usually accompanied by the appearance of several endo- and exothermic peaks in the differential thermograms. However, the interpretation of the DSC and TGA curves in terms of discrete stages with associated weight losses requires a great deal of imagination and certain amount of wishful thinking.

Calculation of thermodynamic activation parameters

The thermodynamic activation parameters of the dehydration and decomposition processes of the investigated samples, such as activation energy ($E^{\#}$), enthalpy ($\Delta H^{\#}$), entropy ($\Delta S^{\#}$), and Gibbs free energy ($\Delta G^{\#}$) were calculated by employing the Coats–Redfern equation [41, 42]:

$$\ln\frac{-\ln(1-\alpha)}{T^2} = -\frac{E}{RT} + \ln\frac{AR}{\theta E^{\#}}, \tag{2}$$

where A is Arrhenius constant, θ is the heating rate, R is the universal gas constant, and α is the fraction of decomposition at temperature T.

A plot of the left-hand side of Eq. 2 against $1/T$ gives a slope, from which $E^{\#}$ was calculated and A was determined from the intercept. The values of $\Delta H^{\#}$, $\Delta S^{\#}$, and $\Delta G^{\#}$ were calculated using the following equations:

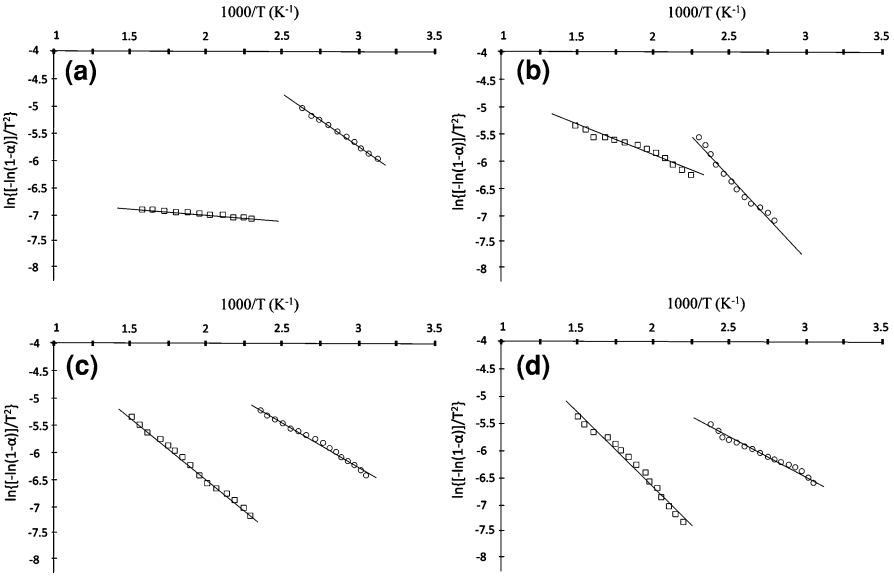

Fig. 6 Coats-Redfern plots of the first (*open circle*) and second (*open square*) degradation steps for **a** pure PVP, **b** pure $Ce(SO_4)_2{\cdot}4H_2O$, **c** PVP + 5 wt% $Ce(SO_4)_2{\cdot}4H_2O$ and **d** PVP + 15 wt% $Ce(SO_4)_2{\cdot}4H_2O$

$$\Delta H^{\#} = E^{\#} - RT, \tag{3}$$

$$\Delta S^{\#} = 2.303\left[\log\frac{Ah}{kT}\right]R, \tag{4}$$

$$\Delta G^{\#} = \Delta H^{\#} - T\Delta S^{\#}, \tag{5}$$

where k and h are Boltzmann and Planck constants, respectively.

Representative Coats–Redfern plots are given in Fig. 6, indicating good correlation for both steps of degradation. The corresponding thermodynamic parameters $E^{\#}$, $\Delta S^{\#}$, $\Delta H^{\#}$, and $\Delta G^{\#}$ are given in Table 2.

The negative entropy values, together with the relatively small values of the thermodynamic activation parameters, indicate the orderness, the relatively low thermal motion, and the relative stability of PVP–$Ce(SO_4)_2{\cdot}4H_2O$ composites for the first degradation step in comparison to the second stage of decomposition.

Conclusions

Newly prepared and well-defined nanocomposite thin films of the system PVP–$Ce(SO_4)_2{\cdot}4H_2O$ were subjected to a follow-up study in order to investigate their structure and thermal behavior within the temperature range 30–400 °C, and to determine some of their thermodynamical characteristics.

X-ray diffraction results revealed that the pure PVP is predominantly amorphous with some localized ordering, i.e., not withstanding the presence of a phase of low regularity. The crystallinity of PVP films increases rapidly with increasing the dopant content up to 15 wt% of $Ce(SO_4)_2{\cdot}4H_2O$ at the expense of the amorphous phase.

The limited solubility of cerium (IV) sulfate tetrahydrate in water restricted the use of dopant concentrations higher than 15 wt%. The estimated average size of the dispersed particles in the investigated composites, as obtained from the X-ray diffraction patterns and confirmed from TEM and AFM images, was found to be within the range of the nanoscale.

DSC and its derivative thermograms indicated that the addition of 2 wt% $Ce(SO_4)_2{\cdot}4H_2O$ to PVP entailed the disappearance of the glass transition peak at 72 °C and the development of a new characteristic endothermic peak at about 240 °C associated with an enthalpy (ΔH) of 49.17 J/g. Both the values of peak position and enthalpy are composition dependent.

TGA and its derivative thermograms revealed that two distinct steps of degradation were clearly evident: one at relatively lower temperature range (30–200 °C), assigned mainly to dehydration processes, and the other at higher temperatures up to 400 °C, attributed mainly to decomposition processes of unspecified nature. The presence of 2–15 wt% $Ce(SO_4)_2{\cdot}4H_2O$ appears to cause an earlier degradation onset than that in pure PVP.

Making use of the thermogravimetric data, some kinetic parameters, including the activation energy E, entropy ΔS, enthalpy ΔH, and the Gibbs free energy ΔG, were determined for the investigated samples. The obtained values of these parameters indicate the orderness, relatively low thermal motion and relative stability of PVP composites in the first stage of degradation when compared to the second stage of decomposition at relatively higher temperatures.

References

1. Sheldon RP (1982) Composite polymeric materials. Elsevier Applied Science, London
2. Sharma AK, Ramu CH (1991) Optical properties of pure and iron-doped cellulose acetate. J Mater Sci Lett 10:1217–1219
3. Anantharaman MR, Malini KA, Sindhu S, Mohammed EM, Date SK, Kulkarni SD, Joy PA, Kurian P (2001) Tailoring magnetic and dielectric properties of rubber ferrite composites containing mixed ferrites. Bull Mater Sci 24(6):623–631
4. Basha AF, Amin M, AbdelSamad HA (1988) Study of thermal currents in vinyl polymers. Indian J Phys 62A:119–129
5. Twomey CJ, Chen SH (1991) Solid polymers doped with rare earth metal salts. I. Complex formation and morphology in the neodymium chloride–poly(ethylene oxide) system. J Polym Sci B 29:859–865
6. Giuffrida S, Condorelli GG, Costanzo LL, Ventimiglia G, DiMauro A, Fragala IL (2008) In situ synthesis of photoluminescent films of PVC, doped with Ce^{3+} ion. J Photochem Photobiol A Chem 195:215–222
7. Abdel Kader FH, Osman WH, Ragab HS, Shehap AM, Rizk MS, Basha MAF (2004) Electrical and optical properties of polyvinyl alcohol thin films doped with metal salts. J Polym Mater 21:49–60
8. Abdel Kader FH, Osman WH, Mahmoud KH, Basha MAF (2008) Dielectric investigations and ac conductivity of polyvinyl alcohol films doped with europium and terbium chloride. Physica B 403:3473–3484
9. Mallinson IC (1987) The foundation of magnetic recording, Chap. 3. Academic Press, Berkeley, CA

10. Oczko G, Macalik L (2010) Optical properties of single crystals of heavy lanthanide chlorides. Polyhedron 29:1231–1236
11. Koechner W (1988) Solid-state laser engineering, 2nd edn. Springer, New York
12. Ao R, Kummerl L, Haarer D (1995) Present limits of data storage using dye molecules in solid matrices. Adv Mater 7:495–499
13. Faria IO, Moreira RL (1999) Dielectric behavior of P(VDF-TrFE)/PMMA blends. J Polym Sci B 37:2996–3002
14. Nagasawa T, Murata Y, Todono K, Kawai R, Kethara KI, Yono S (2000) Dielectric properties of polyarylate blends. J Mater Sci 35:3077–3082
15. Kolekar CB, Kamble PN, Vaingankar AS (1994) Structural and dc electrical resistivity study of Gd^{3+}-substituted Cu-Cd mixed ferrites. J Magn Magn Mater 138:211–215
16. Basha MAF (2010) Magnetic and optical studies on polyvinylpyrrolidone thin films doped with rare earth metal salts. Polym J 42:728–734
17. Basha MAF (2011) Spectroscopic, magnetic and optical characterization of nanocomposite films of polyvinylpyrrolidone doped with cerium disulphate. J Appl Polym Sci. doi:10.1002/app.34295
18. Kumar V, Yang T, Yang Y (1999) Interpolymer complexation. I. Preparation and characterization of a polyvinyl acetate phthalate-polyvinylpyrrolidone (PVAP-PVP) complex. Int J Pharm 188:221–232
19. Jin S, Liu M, Chen S, Gao C (2008) Synthesis, characterization and the rapid response property of the temperature responsive PVP-g-PNIPAM hydrogel. Eur Polym J 44:2162–2170
20. Nishio Y, Haratani T, Takahashi T (1990) Miscibility and orientation behavior of poly(vinyl alcohol) / poly(vinyl pyrrolidone) blends. J Polym Sci Pol Phys 28:355–376
21. Feng J, Weng LT, Chan CM, Xhie J, Li L (2001) Imaging of sub-surface nano particles by tapping-mode atomic force microscopy. Polymer 42:2259–2262
22. Cassu SN, Felisbert MI (1997) Poly(vinyl alcohol) and poly(vinyl pyrrolidone) blends: miscibility, microheterogeneity and free volume change. Polymer 38:3907–3911
23. Holmes RL, Campell JA, Burford RP, Karatchevtseva I (2009) Pyrolysis behaviour of titanium dioxide–poly(vinyl pyrrolidone) composite materials. Polym Degrad Stab 94:1882–1889
24. Casari BM, Langer V (2007) Two $Ce(SO_4)_2.4H_2O$ polymorphs: crystal structure and thermal behavior. J Solid State Chem 180:1616–1622
25. Lindgren O (1977) The crystal structure of cerium(iv) sulfate tetrahydrate, $Ce(SO_4)_2.4H_2O$. Acta Chem Scand A 31:453–456
26. Gabal MA (2009) Effect of Mg substitution on the magnetic properties of NiCuZn ferrite nano-particles prepared through a novel method using egg white. J Magn Magn Mater 321:3144–3148
27. Katainen J, Paajanen M, Ahtola E, Pore V, Lahtinen J (2006) Adhesion as an interplay between particle size and surface roughness. J Colloid Interface Sci 304:524–529
28. ICDD, International Center for Diffraction Data, PDF 01-089-0823
29. ICDD, International Center for Diffraction Data, PDF 00-024-1250
30. Omastova M, Mosnackova K, Trchova M, Konyushenko EN, Stejskal J, Fedorko P, Prokes J (2010) Polypyrrole and polyaniline prepared with cerium(IV) sulfate oxidant. Synth Met 160:701–770
31. Deng Y, Wang L, Yang W, Fu S, Elaissari A (2003) Preparation of magnetic polymeric particles via inverse microemulsion polymerization process. J Magn Magn 257:69–78
32. Artiaga R, Naya S, Garcia A, Barbadillo F, Garcia L (2005) Subtracting the water effect from DSC curves by using simultaneous TGA data. Thermochim Acta 428:137–139
33. Brandrup J, Immergut EH (1975) Polymer handbook, Part III, vol 155. Wiley, New York
34. Griffin-Lewiss O (1968) Physical constants of linear homopolymers. Springer, Berlin, p 128
35. Sidelkovskaye FB (1970) The chemistry of *N*-vinylpyrrolidone and its polymers. Mir, Moscow
36. Van Krevelen DV, Hoftijzer PJ (1972) Properties of polymers, correlation with chemical structure. Elsevier, Amsterdam
37. Caykara T, Demirci S, Kantoglu O (2007) Thermal, spectroscopic, and mechanical properties of blend films of poly(N-vinyl-2-pyrrolidone) and sodium alginate. Polym Plast Technol Eng 46:737–741
38. Udupa MR (1982) Thermal decomposition of cerium(IV), cerium(III), chromium(III) and titanium(IV) sulphates. Thermochim Acta 57:377–381
39. Tagawa H (1984) Thermal decomposition temperatures of metal sulfates. Thermochim Acta 80:23–33
40. Ying Y, Rudong Y (1992) Study on the thermal decomposition of tetrahydrated cerie sulphate. Thermochim Acta 202:301–306
41. Coats AW, Redfern JP (1964) Kinetic parameters from thermogravimetric data. Nature 201:68–69
42. Yakuphanoglu F, Gorgulu AO, Cukurovali A (2004) An organic semiconductor and conduction mechanism: N-[5-methyl-1,3,4-tiyodiazole-2-yl] ditiyocarbamate compound. Physica B 353:223–229